Journal of Engineering Science and Technology
4th EURECA 2015 Special Issue February (2016) 70 - 81

NUMERICAL MODELLING AND EXPERIMENTAL INFLATION VALIDATION OF A BIAS TWO-WHEEL TIRE

CHUNG KET THEIN[1,*], HUEY MEING TAN[2], CHIN HONG LIM[2]

[1]School of Engineering and Physical Sciences, Heriot Watt University Malaysia,
No. 1 Jalan Venna P5/2, Precinct 5, 62200, Putrajaya, Malaysia
[2]School of Engineering, Taylor's University, Taylor's Lakeside Campus,
No. 1 Jalan Taylor's, 47500, Subang Jaya, Selangor DE, Malaysia
*Corresponding Author: ckthein@gmail.com

Abstract

This paper presents a parametric study on the development of a computational model for bias two-wheel tire through finite element analysis (FEA). An 80/90-17 bias two-wheel tire was adopted which made up of four major layers of rubber compound with different material properties to strengthen the structure. Mooney-Rivlin hyperelastic model was applied to represent the behaviour of incompressible rubber compound. A 3D tire model was built for structural static finite element analysis. The result was validated from the inflation analysis. Structural static finite element analysis method is suitable for evaluation of the tire design and improvement of the tire behaviour to desired performance. Experimental tire was inflated at various pressures and the geometry between numerical and experimental tire were compared. There are good agreements between numerical simulation model and the experiment results. This indicates that the simulation model can be applied to the bias two-wheel tire design in order to predict the tire behaviour and improve its mechanical characteristics.

Keywords: Bias tire, Finite element analysis, Footprint test.

1. Introduction

Tire is a component which allows interaction between a road surface and a vehicle. Its main function is to allow steering control for the vehicle to travel to intended destination and to support load of vehicle and passenger. Bias two-wheel tire is commonly used for underbone motorcycles in Malaysia and its construction consists of multiple layers as shown in Fig. 1. Bias two-wheel tire consists of 4 major components which are the tread, tread base, cord-rubber plies, and inner

Nomenclatures

d	volumetric response constant
I	strain invariant
I_1	First deviatoric
I_2	Second deviatoric
J	ratio of compressed volume to uncompressed volume
W	strain energy density function

Greek Symbols

λ	stretch ratio

Abbreviations

FEA	Finite element analysis

liner. The cord-rubber plies which are made up of twisted Nylon-6 cord and rubber compound are arranged on bias at an angle within the range of 25˚ to 40˚ [1]. Bias tire provides smoother ride on rough and uneven surfaces as the construction structure is strong and has stiffer sidewall with softer tread which can be flexed easily.

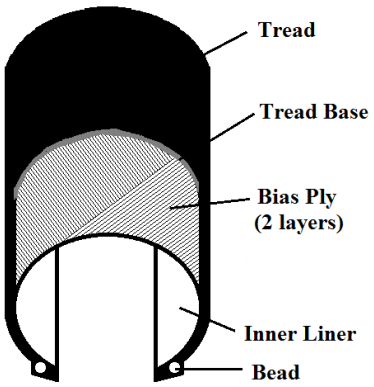

Fig. 1. Components of bias tire.

In this paper, an 80/90-17 bias two wheel tire was chosen. It has section width of 80 mm and an aspect ratio of 90%. This means that the section height of the tire is a 0.9 factor of 80 mm, which is 72 mm and the 17 represent the rim diameter in inch. Tire is inflated to a standard pressure allocated based on the load index of 44 and the speed rating P. The tire should be inflated to a pressure of 230 kPa as this is the standard inflation pressure for this type of tire [2]. Measurements on the tire geometry will be conducted after inflation to check on the dimension of the tire as compared to its intended design.

Experimental tires can be manufactured based on various parameters to observe the effect on the tire geometry after inflation test. However, to reduce the experimental cost and time, computer simulation is opted. In this paper, the main objective is to develop a computational tire model for finite element analysis

(FEA) which can predict the behavior of the bias two-wheel tire under different condition of load and pressure.

This paper focused on static loading on the bias two-wheel tire and its effects on the geometry of the tire; before and after inflation. As described by Korunovie et al. [3], axisymmetric tire model is enough to show good correlation between the analysis results with the experimental results. In addition, Mohsenimanesh et al. [4] also reported that the computational modelling of axisymmetric tire models on the inflation pressure has higher effect on the contact area of the tire compared to the load on a rigid surface. These tire models are focused on car and truck tires but little research is carried out for bias two-wheel tire for the motorcycles.

FEA is a common alternative to the expensive and time-consuming physical prototyping for new tire designs. Thus, detailed modelling of the tire structure is necessary to allow higher accuracy in predicting the behavior of the future tire. One of the major criteria is to describe the material behavior of structural tire components accurately. The Mooney-Rivlin hyperelastic material model is applied in this study to represent the material properties of rubber compound of the bias two-wheel tire. The Mooney-Rivlin model is employed due to the material model stability and it is commonly used for other researchers which have proven to yield results with minor discrepancies. Several researchers have managed to model tires by adopting incompressible Mooney-Rivlin material model and have generated FEA tire model with results that are comparable to the experimental tires [3, 5, 6]. In addition, Mooney-Rivlin hyperelastic model is suitable as deformations in tire rarely reaches 40% during its service, as mentioned by Tönük [7]. Therefore, this method is applied for the modelling of two-wheel bias tire.

Static analysis is primarily applied in this study to check the validity of the FEA bias two-wheel tire model. In the following sections, the detailed modelling of the tire is presented.

2. Methodology

The 80/90-17 bias two-wheel tire is a composite material consists of mainly four layers which are the tread, tread base, cord-rubber plies, and inner liner. The cord-rubber plies are made up of high modulus cord and low modulus rubber; with twisting threads of Nylon-6 made up the cord. Each layer of the tire is made up of rubber compound with different material properties. Hence, determination of the material properties of the rubber compound is important to ensure proper settings for the FEA simulations. In the following sections, the methods to estimate the material properties of each layer are described. The modelling of tire model through FEA software is also explained in detail.

2.1. Determination of Mooney-Rivlin constants

Mooney-Rivlin is a hyperelastic model which is commonly used to represent the material properties of rubber compound. In this study, the rubber compounds that made up the bias ply two-wheel tire are assumed to be incompressible. The strain-energy density function for hyperelastic materials can be represented in Eq. (1).

$$W = \sum_{i=0,\, j=0}^{N} C_{ij}\left(\overline{I_1} - 3\right)^i \left(\overline{I_2} - 3\right)^j + \sum_{k=1}^{N} d_k \left(J - 1\right)^{2k} \tag{1}$$

where C_{ij} is the constants for distortional response, d is the volumetric response constant, and J is the ratio of compressed volume to uncompressed volume. In the case of incompressibility, the J value is 1. Parameters i, j, and k represents the direction of the material response in three different directions within the three-dimensional space.

From Eq. (1), the strain energy density function, W is expressed in terms of strain invariant I, where I_1 and I_2 are the first and second deviatoric strain invariants. Strain invariant I can be represented in terms of stretch ratio, λ as shown in Eq. (2). The relation between $\overline{I}_1$ and $\overline{I}_2$ with J are shown in Eqs. (3) and (4).

$$I_1 = \lambda_1^2 + \lambda_2^2 + \lambda_3^2$$
$$I_2 = \left(\lambda_1\lambda_2\right)^2 + \left(\lambda_2\lambda_3\right)^2 + \left(\lambda_1\lambda_3\right)^2 \tag{2}$$
$$I_3 = \left(\lambda_1\lambda_2\lambda_3\right)^2$$
$$\overline{I}_1 = J^{-2/3} I_1 \tag{3}$$
$$\overline{I}_2 = J^{-4/3} I_2 \tag{4}$$

Polynomial form of the strain energy function Eq. (1) for hyperelastic model is the general form for Mooney-Rivlin model. In this study, 5-parameters Mooney-Rivlin model is applied. It is a better representation of the stress-strain response at larger values of stretch compared to 2-parameters or 3-parameters Mooney-Rivlin hyperelastic model [8].

Extending Eq. (1) to the second order term where N=2 leads to the 5-parameters Mooney-Rivlin model strain energy density function as shown in Eq. (5).

$$W = C_{10}(I_1 - 3) + C_{01}(I_2 - 3) + C_{20}(I_1 - 3)^2 + C_{11}(I_1 - 3)(I_2 - 3) + C_{02}(I_2 - 3)^2 \tag{5}$$

where C_{10} and C_{01} terms describe the shear behavior of the material. C_{20}, C_{11}, and C_{02} were the additional higher order terms to provide good curve fit for the Mooney-Rivlin strain energy function in the Eq. (5). The strain energy equation is a representation of the stress-strain relationship of a rubber compound. Various types of experiment such as the uniaxial tensile testing, biaxial test, planar or pure shear test, and volumetric test can be executed to estimate the rubber material properties through the Mooney-Rivlin hyperelastic model.

In this study, uniaxial tension testing was carried out to determine the stress-strain behavior of rubber compound for different layers of the bias two-wheel tire.

2.1.1. Uniaxial tension test

Uniaxial tension test is executed to determine the material properties of each layer of rubber compound for the bias two-wheel tire. The rubber compounds were cured into standard ring shape with diameter of 44 mm and external diameter of 53 mm, at a thickness of 6 mm. The rubber ring was positioned on the tensiometer pulleys and

pulled until rupture. Figure 2 shows that the equipment used in this test was a tensile testing device with pulleys for mounting the test specimen.

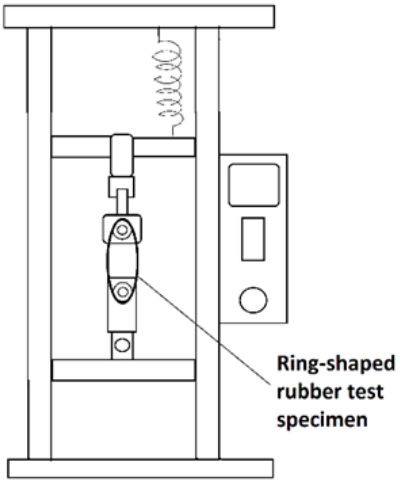

Fig. 2. Ring testing machine.

The uniaxial tension testing is carried out at surrounding temperature of 23°C, no earlier than 16 hours after vulcanization. The driven pulley made one revolution for every 50 mm linear motion of the tensioning head. One side of the pulley is driven while the other is free-wheeling. The speed of the pulley was 500 mm/min and three rings were tested for each layer of the rubber compound of the bias two-wheel tire. The test machine is under remote computer control to record the testing results.

Strain invariants of each layer of the rubber compound can then be determined based on the testing results. Material constants for the Mooney-Rivlin hyperelastic model were then predicted through curve fitting using ANSYS Workbench. Experimental stress-strain data were fit according to the hyperelastic model to estimate the material constants of C_{10}, C_{01}, C_{20}, C_{11}, and C_{02}. Similar technique was applied to gather Mooney-Rivlin constants for the tread base, and inner liner. The material constants obtained from the curve fitting were tabulated in Table 1.

Table 1. Hyperelastic material constants.

Rubber Material (Compounds)	Material Constants of Mooney-Rivlin Strain Energy Potential (MPa)				
	C_{10}	C_{01}	C_{20}	C_{11}	C_{02}
Tread	-3.6500	5.5300	0.01350	0.0452	1.2700
Tread Base	-5.5400	9.1600	-0.35900	1.9900	0.1060
Inner Liner	-3.3700	5.2300	0.00494	0.1010	1.1900

2.2. Cord-Rubber layer Rebar model

Tire has complex characteristics as it is a product of composite materials. The cord-rubber plies that are made up of rubber compound and reinforced with

twisting threads of Nylon-6 were modelled using rebar model to estimate the material properties at these layers. Figure 3 shows that the rebar model was setup for uniaxial tensile testing simulations.

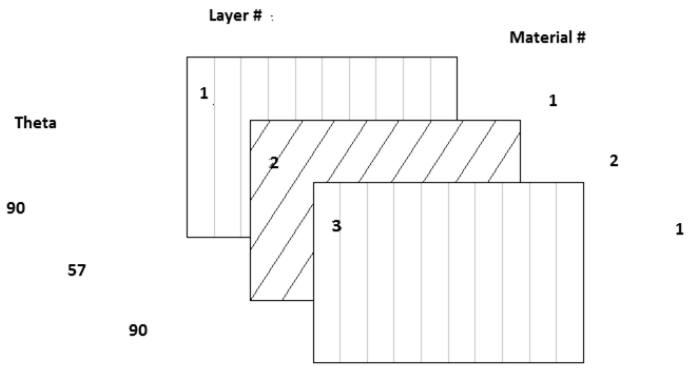

Fig. 3. Rebar model for uniaxial tensile testing.

SHELL181 was applied in the simulation for the element of the rebar model, followed by orientation angle setting of 90˚ for rubber compound layer and 57˚ for the cord layer. Then, forces were applied in the vertical x-direction to the rebar model as shown in Fig. 4. From the simulation, the stress strain values can be determined by graduate increase the force applied. Thus, the material constant of the Mooney-Rivlin for cord-rubber ply can be predicted through the curve fitting from ANSYS Workbench. Table 2 shows the Mooney-Rivlin material constants for the cord-rubber ply.

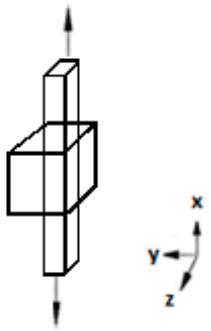

Fig. 4. Uniaxial tension testing.

Table 2. Hyperelastic material constant for cord-rubber ply.

Rubber Material (Compounds)	Material Constants of Mooney-Rivlin Strain Energy Potential (MPa)				
	C_{10}	C_{01}	C_{20}	C_{11}	C_{02}
Cord-Rubber Ply	-1.8400	3.3200	0.01690	0.1330	0.5820

2.3. Tire model

The 80/90-17 bias ply two-wheel tire was modelled using ANSYS. The detail modelled of the tire was shown in Fig. 5.

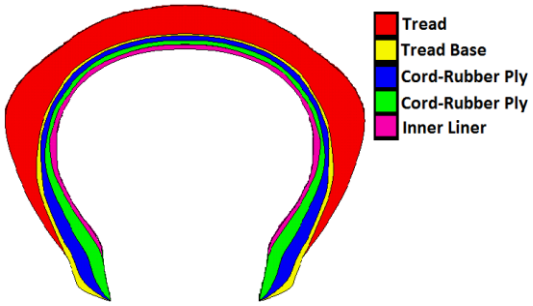

Fig. 5. 3D Model for the bias two-wheel tire.

The tire is constructed according to the cross section geometry and tire specifications for the 80/90-17 bias ply two-wheel tire. There were 5 layers and each individual layer was set to be SOLID186 which is a 20-node solid element that exhibits quadratic displacement with 3 degree-of-freedom per node that supports hyperelasticity. The tire was modelled to 20-degree to reduce computational time by decreasing the number of elements and nodes.

The bias two-wheel tire 3D model is assumed to be symmetrical along its neutral axis and inflation pressure was set to simulate inflation process similar to the real inflation process on experimental tire. Fixed displacement was set on the area of the tire where it was mounted on the rim. The boundary conditions were set for the 3D tire model to represent inflation test as shown in Fig. 6. The rim is considered to be negligible as the fixed displacement is applied.

Convergence test was perform to check the mesh density and comparisons were made to determine the most suitable mesh size for tire model as shown in Fig. 7. From Fig. 7, the minimum displacement is recorded around 4.883 mm with approximately 17,500 elements for the 20-degree modelled. This was corresponding to the element size of 1.15 mm. This element size is unsuitable to use as the smallest thickness layer tire is approximately 1 mm. Thus, 1 mm hexahedral element with 19566 elements was selected to generate the model which is shown in Fig. 8.

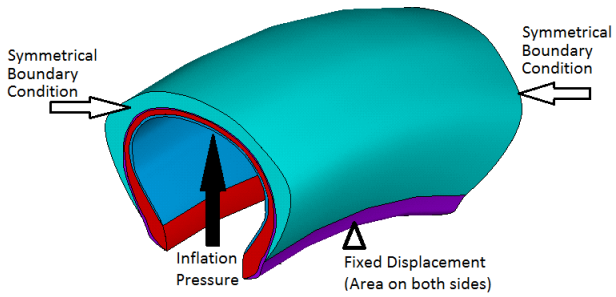

Fig. 6. Boundary condition of 3D tire model (20-degree).

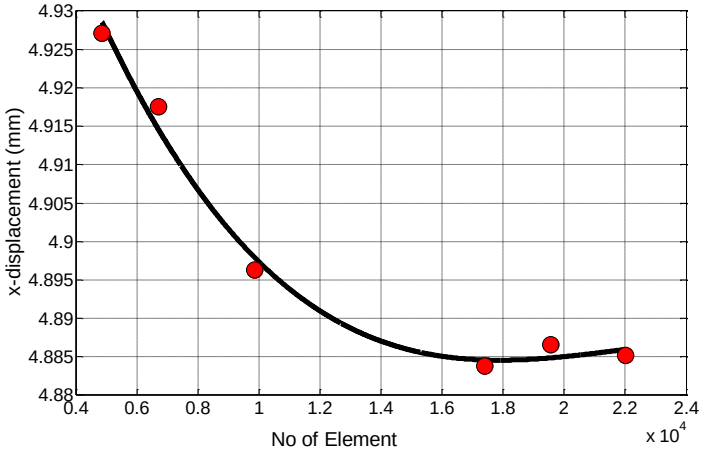

Fig. 7. Convergence test using x-displacement at various element numbers.

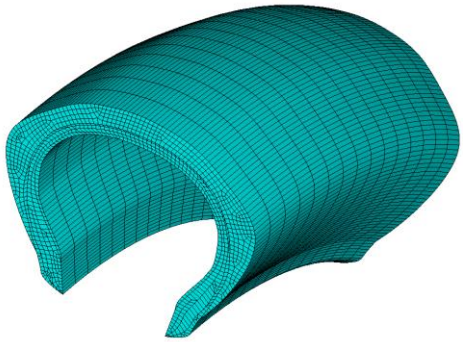

Fig. 8. Mesh element of FEA model.

3. Results and Discussions

The tire model's response of the inflation test was promising. The tire was inflated to the maximum capacity of 270 kPa, representing a 42% increase in the tire's rated inflated pressure of 190 kPa. Validation on the FEA tire model was carried out through inflation test. Experimental bias two-wheel tire was mounted on a tire rim and inflated to the standard inflation pressure of 230 kPa, in accordance to the speed rating at the maximum load of the tire. Measurements were carried out on the mounted tire after the tire was conditioned to room temperature of 27˚C for 3 hours. This was the standard procedure carried out by the tire manufacturer.

The diameter of the experiment tire was measured using special equipment. However, for the simulation, the diameter can be easily obtained from the analysis. Thus, the tire diameter was calculated using Eq. (6).

$$D_{FEA} = D_{P(0)} + 2d_x \tag{6}$$

where D_{FEA} is the FEA tire model diameter; $D_{P(0)}$ is the tire diameter before inflation; and d_x is the displacement deformation in x-direction. Figure 9 shows

that the comparison of the outside diameter for the experiment and the numerical solution. The vertical displacement of the inflated tire at 230 kPa is shown in Fig. 10.

As the inflation pressure increased, the diameter of the tire increased for both experimental bias two-wheel tire and the FEA tire model. This could be expected as the elements used for the cord-rubber layer are assumed to be a uniform layer with constant behavior. In the experimental tire, each cord integrated in the cord-rubber layer changed its position with respect to the deformation of tire at different direction. The exact orientation of the cord is not the focus in this study. Thus, the analysis results are considered to be in a good agreement between the experimental tires and simulation model which is approximately differ by 0.36% to 0.62%. Figure 11 shows that the location of the section width. The inflated test was further analysing its section width as shown in Fig. 12.

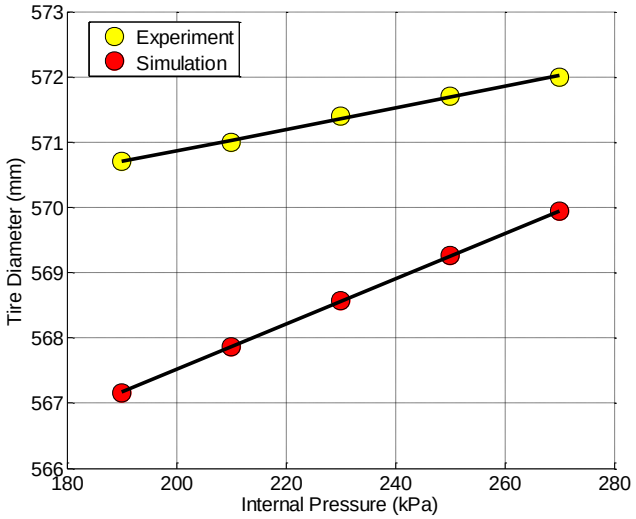

Fig. 9. Comparisons of experimental tire and simulation results.

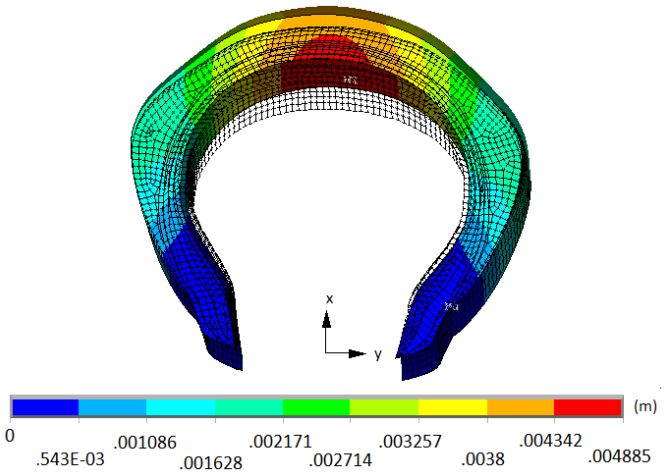

Fig. 10. Vertical displacement deformation (x-direction): initial deformation (wire frame) and final deformation at pressure 230 kPa.

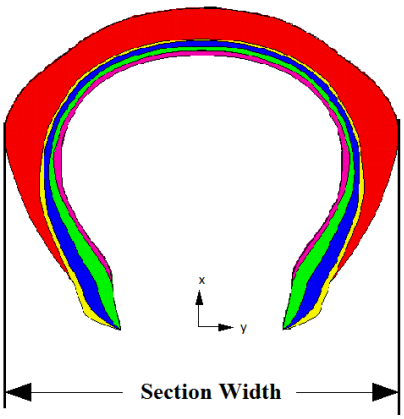

Fig. 11. Section width.

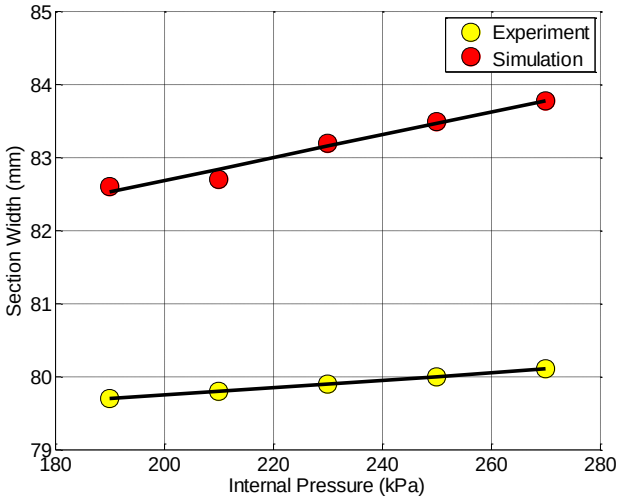

Fig. 12. Bias tire section width.

For the section width, the tire expanded in terms of width for both experimental tire and finite element tire model. The predicted section width displacement by the finite element tire model correlates reasonably with the experimental bias two-wheel tire with maximum discrepancy of 4.6%. The minor difference between the experimental tire and finite element tire model is expected as the cord-rubber layers were assumed to be uniform layer with constant behaviour. However, in experimental bias two-wheel tire, there were twisting cords integrated in the cord-rubber layer which will affect the deformation behaviour of the tire. Thus, the analysis results are considered to be in good correlation between the experimental bias two-wheel tire and the finite element tire model. Internal deformation of the cord-rubber ply could have resulted in the differences between the experimental tire and FEA tire model.

In order to further understand the behaviour of the bias tire, the tire stress distribution was analysed. Figure 13 is the von-Mises stress of the bias tire at internal pressure of 230 kPa.

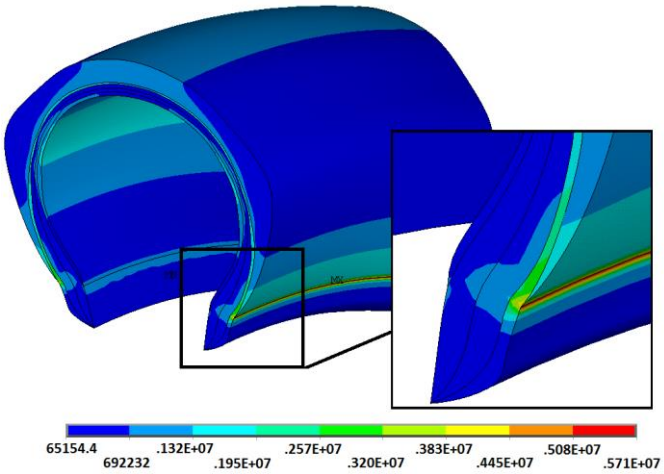

Fig. 13. Von-Mises stress of the bias tire (MPa).

Figure 13 shows that the maximum stress occurs at the edge where the rim is attached. The stress can be further reduced by strengthen it with higher strength of material which will be embedded inside the tire. From Fig. 13, most of the stresses are occurred less than 2 MPa. In order to visualise the stress distribution of each layer, the scale of maximum von-Mises stress is set to a maximum of 2 MPa, as shown in Fig. 14.

Figure 14 shows that the maximum stresses occur at the thread base and the inner liner are higher compare to the other layers. This is because the material constant for thread base and inner liner are lower than others due to the low modulus of elasticity. Hence, the material constants of thread base and inner liner are smaller as shown in Table 1.

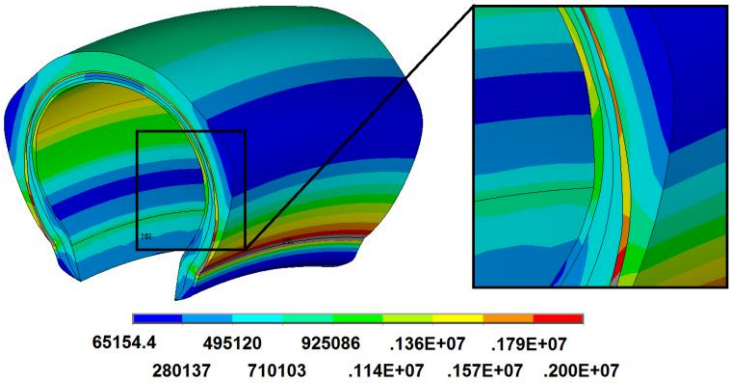

Fig. 14. von-Mises stress (MPa) (Maximum value is set to 2 MPa).

4. Conclusions

The geometry of the tire during the inflation process is compatible between the real experimental tire and the FEA tire model of bias two-wheel tire. There is minor discrepancy for the inflation test where the different inflation pressure was applied on the tire. The results of static loading on the FEA tire model shown in this paper indicate that this tire model is successfully developed in order to predict the bias two-wheel tire behavior during inflation test. FEA method is important as it reduces the cost and time required for designer to explore on a variety of designs.

On top of that, the FEA tire model can be used to tune and optimize the current performance of the tire. It is also possible to observe and evaluate possible effects on tire durability. Future work will be conducted on the footprint contact area to further analyse the contact pressure distribution.

Acknowledgment

The experiments in this paper are supported by Continental Tyre Malaysia Sdn. Bhd. The authors would also like to thank all the persons that involved in this research.

References

1. Nakasaki, E. (1976) United States Patent 1191 US. Patent. 1-6
2. T.E.T.; and R.T. (2014). Organisation, *ETRTO Standards Manual 2014*. Brussels. M1-M12.
3. Korunović, N.; Trajanovć, M.; and Stojković,, M. (2007). FEA of tyres subjected to static loading. *Journal of the Serbian Society for Computational Mechanics*, 1(1), 87-98.
4. Mohsenimanesh, A.; Ward, S.M.; Gilchrist, M.D. (2009). Stress analysis of a multi-laminated tractor tyre using non-linear 3D finite element analysis. *Materials & Design*, 30(4), 1124-1132.
5. Watanabe, Y.; and Kaldjian, M.J. (1985). Modeling and analysis of bias-ply motorcycle tires. *Mathematical Modelling*, 6(1), 80.
6. Cheng, G.; Zhao, G.; Guan, Y.; and Wang, Z. (2011). Study on deflection performance of radial Tire by finite element method. *Noise and Vibration Worldwide*, 42(11), 30-35.
7. Tönük, E. (1998). *Computer simulation of dynamic behaviour of pneumatic tires*. Ph.D. Thesis, Middle East Technical University, Ankara.
8. Sasso, M.; Palmieri, G.; Chiappini, G.; and Amodio, D. (2008) Characterization of hyperelastic rubber-like materials by biaxial and uniaxial stretching tests based on optical methods. *Polymer Testing*, 27(8), 995-1004.